IEEE Access
Multidisciplinary | Rapid Review | Open Access Journal

Received July 2, 2018, accepted August 22, 2018, date of publication September 13, 2018, date of current version October 12, 2018.

Digital Object Identifier 10.1109/ACCESS.2018.2869991

Field-Oriented Control of Energy-Regenerative Electromagnetic Slip Coupling

BIN TANG[1], YINGQIU HUANG[2], DI ZHANG[2], HAOBIN JIANG[2], YINGFENG CAI[1], AND XIAODONG SUN[1], (Member, IEEE)

[1]Automotive Engineering Research Institute, Jiangsu University, Zhenjiang 212013, China
[2]School of Automotive and Traffic Engineering, Jiangsu University, Zhenjiang 212013, China

Corresponding author: Bin Tang (tangbin@ujs.edu.cn)

This work was supported in part by the National Natural Science Foundation of China under Grant 51605199 and Grant 51275211, in part by the Natural Science Foundation of Jiangsu Province under Grant BK20160527, in part by the China Postdoctoral Science Foundation under Grant 2016M590417, in part by the Natural Science Foundation for Colleges and Universities of Jiangsu Province under Grant 16KJB580001, in part by the Postdoctoral Science Foundation in Jiangsu Province under Grant 1601222C, and in part by the Scientific Research Foundation of Jiangsu University under Grant 15JDG093.

ABSTRACT Electromagnetic slip coupling (EMSC), like other contactless transmission devices, has lots of advantages over contact transmissions such as clutch function, continuous speed regulation, and no mechanical wear. Nevertheless, the EMSC has inherent slip energy especially under the large-slip condition, which leads to low efficiency. A novel energy-regenerative EMSC was developed including wound-type EMSC and the energy-regenerative apparatus for slip energy recovery. To improve recovery efficiency of the EMSC, the field-oriented control strategy was proposed. In this case, the mathematical model of EMSC under synchronously rotating coordinate system was constructed and verified by experiment. Since direct-axis component and quadrature-axis component of current in three-phase windings of the EMSC are coupled, the feed forward decoupling control approach was employed. Space vector pulse width modulation technique was utilized to eliminate harmonic components of current in three-phase windings. Simulations and experiments were carried out to validate the proposed control strategy. The results showed that the voltage and current in three-phase windings were almost in-phase, the current only contained few of harmonic components, and slip energy of the EMSC decreased by 82.5%. In conclusion, the field-oriented control strategy is conducive to recycle the slip energy of the EMSC efficiently.

INDEX TERMS Electromagnetic slip coupling, energy-regenerative, energy recovery efficiency, field-oriented control, PWM rectifier, space vector pulse width modulation.

I. INTRODUCTION

In modern industries, variable frequency motors have been widely used in drive and transmission applications [1]–[3]. Nevertheless, they are not applied in the area of unavailable electric power, such as automotive transmission, ship propulsion and construction machinery, where mechanical load can be adjusted by the coupling equipped between prime mover and mechanical load. There are generally three types of couplings, respectively, mechanical coupling [4], [5], hydraulic coupling [6], [7], and magnetic coupling [8], [9] among which magnetic coupling is more reliable and feasible because of no mechanical wear and oil pollution. Magnetic couplings are classified as electromagnetic slip coupling (EMSC) [10], [11] and permanent magnetic coupling [12], [13] according to different ways of excitation. In terms of variable speed transmission, EMSC varies speed of mechanical load by controlling excitation current, while permanent magnetic coupling adjusts speed of mechanical load by varying length or area of the air gap via a mechanism [14] which is more complicated.

EMSC transmits power through the interaction between excitation field generated by excitation current and induction field generated by eddy current [15]. Due to the eddy current, the slip energy, that is energy difference between the input and output of EMSC, dissipates as heat, which results in low efficiency especially under large-slip conditions [16]. To improve transmission efficiency of EMSC the slip energy should be recycled. One of feasible approaches is to conduct eddy current out of the armature by three-phase windings. The induced current in three-phase

windings should be converted to direct current (DC) before slip energy recovery. Conventional rectifiers that convert alternating current into direct current are diode rectifier and silicon controlled rectifier, respectively constituted of diodes and thyristors [17], [18]. For silicon controlled rectifier, phase of the input current lags behind phase of the input voltage and the phase hysteresis increases with the trigger angle of thyristor. So power factor of silicon controlled rectifier is relatively low, which indicates low efficiency [19]. For diode rectifier, although the phase hysteresis between input voltage and input current is nearly zero, input current contains large numbers of high-frequency harmonic components which also result in low power factor [20]. PWM rectifier, whose input current is sinusoidal and in-phase with the input voltage, can realize unity power factor [21]–[23].

Field-oriented control has been widely applied in three-phase motors [24]–[27]. Based on field-oriented control theory [28], direct-axis component of the induced three-phase current tracks the target value of zero to realize synchronization between input current and input voltage of the PWM rectifier. For modulation of the PWM rectifier, space vector pulse width modulation (SVPWM) is superior to sinusoidal pulse width modulation (SPWM) in some aspects, such as high voltage utilization ratio, low switching frequency and easy implementation [29], [30], so SVPWM technique is applied to ensure that input current of the PWM rectifier is sinusoidal, thus improve dynamical performance. After rectification, the slip energy in the form of direct current is recycled by the super capacitor that is widely used in energy storage system [31]–[33] because of its high power density and longer cycle lifetime [34].

II. CONFIGURATION OF ENERGY-REGENERATIVE EMSC

The energy-regenerative EMSC is a dual mechanical ports machine, which consists of outer rotor, inner rotor, and energy-regenerative apparatus, as shown in FIGURE 1. Outer rotor and inner rotor are embedded with three-phase windings and field winding respectively. Outer rotor connects to prime mover by the input shaft, and inner rotor connects to mechanical load by the output shaft. The energy-regenerative apparatus including PWM rectifier, super capacitor and controller recycles slip energy in three-phase windings. The controller regulates current of the field winding and modulates PWM rectifier. When the outer rotor is driven by the prime mover, the three-phase windings induce three-phase alternating current under the excitation of magnetic field generated by field winding. Due to the interaction between induction field and excitation field, the inner rotor rotates along with outer rotor in asynchronous speed. The PWM rectifier converts induced alternating current into direct current to charge the super capacitor for slip energy recovery.

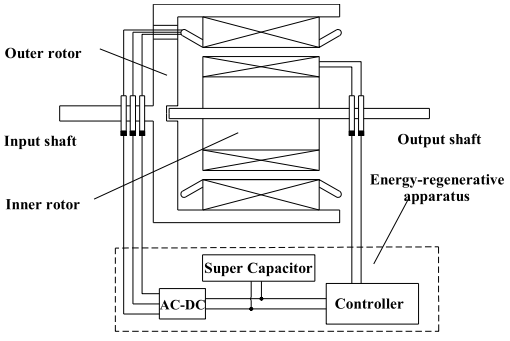

FIGURE 1. Configuration of energy-regenerative EMSC.

III. MATHEMATICAL MODEL

A. MODEL OF EMSC

The developed EMSC prototype includes thirty-six slots and three pairs of magnetic poles. Due to time-variant self-inductance and mutual inductance of three-phase windings and field winding under fixed coordinate system (a-b-c coordinate) [35], mathematical model of the EMSC is constructed under synchronously rotating coordinate system (d-q coordinate). Taking no account of flux saturation, harmonic wave and armature reaction, flux linkage equations, terminal voltage equations, electromagnetic torque equation and kinematic equations are established, shown as follows.

$$\begin{cases} \psi_d = L_d i_d + M_{sf} i_f \\ \psi_q = L_q i_q \\ \psi_f = L_f i_f + \dfrac{3}{2} M_{sf} i_d \end{cases} \tag{1}$$

$$\begin{cases} u_d = -\dfrac{d\psi_d}{dt} - R_s i_d + \omega \psi_q \\ u_q = -\dfrac{d\psi_q}{dt} - R_s i_q - \omega \psi_d \\ u_f = R_f i_f + \dfrac{d\psi_f}{dt} \end{cases} \tag{2}$$

$$T_e = \frac{3}{2} n_p i_q \left[(L_d - L_q) i_d + M_{sf} i_f \right] \tag{3}$$

$$\begin{cases} T_i = J_1 \dfrac{d\Omega_1}{dt} + B_1 \Omega_1 + T_e \\ T_e = J_2 \dfrac{d\Omega_2}{dt} + B_2 \Omega_2 + T_L \end{cases} \tag{4}$$

Where, ψ_d is direct-axis component of flux linkage of three-phase windings, ψ_q is quadrature-axis component of flux linkage of three-phase windings, L_d is direct-axis component of self-inductance of three-phase windings, L_q is quadrature-axis component of self-inductance of three-phase windings, L_f is self-inductance of field winding, M_{sf} is mutual inductance between three-phase windings and field winding, i_d is direct-axis component of current in three-phase windings, i_q is quadrature-axis component of current in three-phase windings, u_d is direct-axis component of terminal voltage of three-phase windings, u_q is quadrature-axis component of terminal voltage of three-phase windings, i_f is excitation current of field winding, u_f is terminal voltage of field winding, R_s is resistance of each phase winding in outer rotor, R_f is resistance of field winding in inner rotor, ω is electrical angular velocity difference between outer rotor and inner rotor, n_p is pole pairs of inner rotor, T_i is drive torque on outer rotor, T_e is electromagnetic torque, T_L is load

torque on inner rotor, J_1 is rotational inertia of outer rotor, J_2 is rotational inertia of inner rotor, B_1 is viscous damping coefficient of outer rotor, B_2 is viscous damping coefficient of inner rotor, Ω_1 is mechanical angular velocity of outer rotor, Ω_2 is mechanical angular velocity of inner rotor.

TABLE 1. Simulation parameters of EMSC.

Parameters /unit	value
Self-inductance of direct -axis L_d/H	8.5e-3
Self-inductance of quadrature -axis L_q/H	5.5e-3
Mutual inductance M_{sf}/H	20e-3
Pole pairs of inner rotor n_p	3
Resistance of three-phase windings R_s /Ω	2e-1
Resistance of field winding R_f/Ω	3e-1
Rotational inertia of inner rotor J_2 /kg·m^2	1e-2
Viscous damping coefficient B_2 /N·m/rad/s	5e-3

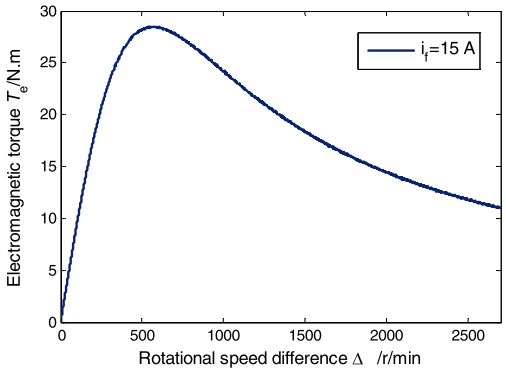

FIGURE 2. Dynamic characteristic.

The simulation model of EMSC in Matlab/Simulink is built, and its parameters are shown in TABLE 1. The dynamic characteristic, mechanical characteristic, output speed versus input speed characteristic, and output speed versus excitation current characteristic are simulated. The simulation results are shown in FIGURE 2 to FIGURE 5. In FIGURE 2, as the rotational speed difference increases, the electromagnetic torque first increases linearly and then decreases dramatically, which demonstrates that mechanical characteristic of the uncontrolled EMSC is soft. In FIGURE 3, the mechanical characteristic presents the linearity at the rotational speed range from 0 to 600 r/min, which is consistent with the dynamic characteristic. In FIGURE 4, output speed of the EMSC varies linearly with input speed. In FIGURE 5, output speed of the EMSC varies dramatically with excitation current, which also indicates that mechanical characteristic of the uncontrolled EMSC is flexible. The experiments about mechanical characteristic, output speed versus input speed characteristic and output speed versus excitation current characteristic were carried out to verify mathematical model of the EMSC. The comparisons of simulation and

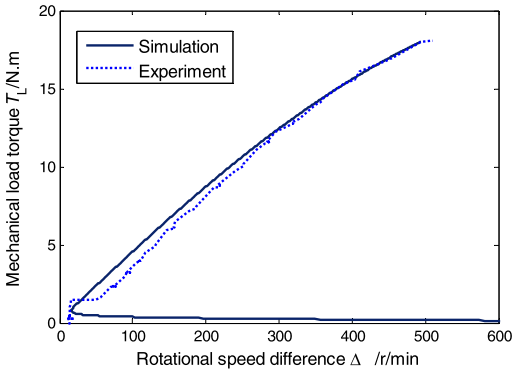

FIGURE 3. Mechanical characteristic.

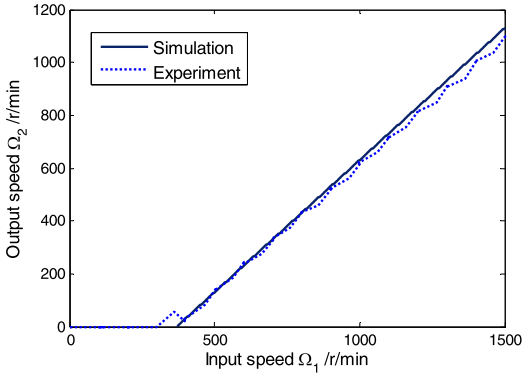

FIGURE 4. Output speed versus input speed characteristic.

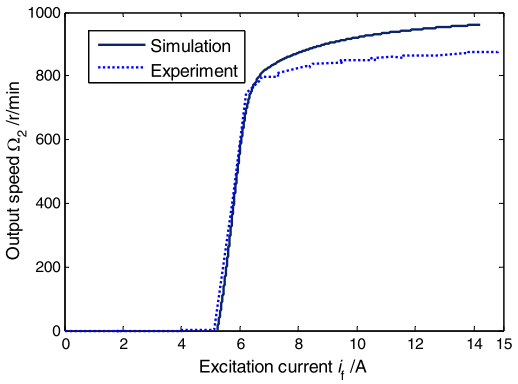

FIGURE 5. Output speed versus excitation current characteristic.

experiment results are implemented as shown in FIGURE 3 to FIGURE 5. It can be seen that simulation results are consistent with the experiment results, which demonstrates that the model of EMSC is correct and precise.

B. MODEL OF PWM RECTIFIER

The PWM rectifier includes three pairs of MOSFETs, filter inductors and super capacitor as shown in FIGURE 6.

Mathematical model of the PWM rectifier is built based on Kirchhoff voltage law and Kirchhoff current law, shown

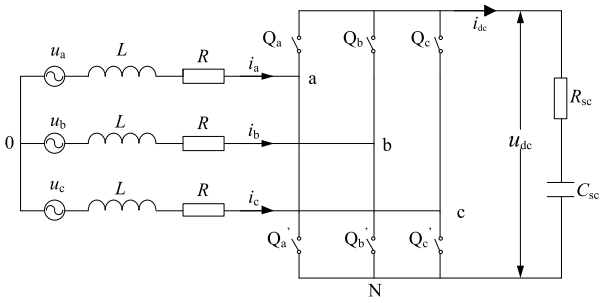

FIGURE 6. Schematic of PWM rectifier.

as following equations.

$$\begin{cases} L\dfrac{\mathrm{d}i_a}{\mathrm{d}t} = u_a - Ri_a - (S_a - \dfrac{S_a+S_b+S_c}{3})u_{dc} \\ L\dfrac{\mathrm{d}i_b}{\mathrm{d}t} = u_b - Ri_b - (S_b - \dfrac{S_a+S_b+S_c}{3})u_{dc} \\ L\dfrac{\mathrm{d}i_c}{\mathrm{d}t} = u_c - Ri_c - (S_c - \dfrac{S_a+S_b+S_c}{3})u_{dc} \\ u_{dc} = (S_a i_a + S_b i_b + S_c i_c)R_{sc} \\ \qquad + \dfrac{1}{C_{sc}}\displaystyle\int (S_a i_a + S_b i_b + S_c i_c)\mathrm{d}t \end{cases} \tag{5}$$

Where, L is inductance of filter inductor, R is equivalent resistance of filter inductor and MOSFETs, S_a, S_b and S_c are switch functions that indicate the states of rectifier bridge arms, i_a, i_b, i_c are input current of rectifier bridge, u_a, u_b, u_c are input voltage of rectifier bridge, u_{dc} is voltage of DC side after rectification, C_{sc} is capacitance of super capacitor, R_{sc} is internal resistance of super capacitor.

Through Clarke-Park transformation, model of PWM rectifier is deduced under d-q coordinate system as shown in expression (6).

$$\begin{cases} L\dfrac{\mathrm{d}i_d}{\mathrm{d}t} = u_d - Ri_d - S_d u_{dc} + L\omega i_q \\ L\dfrac{\mathrm{d}i_q}{\mathrm{d}t} = u_q - Ri_q - S_q u_{dc} - L\omega i_d \\ u_{dc} = \dfrac{3}{2}(i_d S_d + i_q S_q)R_{sc} + \dfrac{3}{2C_{sc}}\displaystyle\int (i_d S_d + i_q S_q)\mathrm{d}t \end{cases} \tag{6}$$

Where, S_d is direct-axis component of switch value of rectifier bridge arms, S_q is quadrature-axis component of switch value of rectifier bridge arms.

C. INTEGRATED MODEL OF EMSC AND PWM RECTIFIER

From the structure of the energy-regenerative EMSC, it can be seen that three-phase windings in outer rotor connect with PWM rectifier, thus current in three-phase windings is also the input current of PWM rectifier.

By combining expression (1), (2) and (6), integrated model of EMSC and PWM rectifier is deduced as follows.

$$\begin{cases} (L_d + L)\dfrac{\mathrm{d}i_d}{\mathrm{d}t} = -(R_s + R)i_d + (L_q + L)\omega i_q \\ \qquad\qquad - M_{sf}\dfrac{\mathrm{d}i_f}{\mathrm{d}t} - S_d u_{dc} \\ (L_q + L)\dfrac{\mathrm{d}i_q}{\mathrm{d}t} = -(R_s + R)i_q - (L_d + L)\omega i_d \\ \qquad\qquad - M_{sf}\omega i_f - S_q u_{dc} \\ u_{dc} = \dfrac{3}{2}(i_d S_d + i_q S_q)R_{sc} + \dfrac{3}{2C_{sc}}\displaystyle\int (i_d S_d + i_q S_q)\mathrm{d}t \end{cases} \tag{7}$$

IV. CONTROL STRATEGY

The control aim is to recycle slip energy efficiently and improve dynamical performance of the EMSC. From the kinematic equations of the EMSC, it can be seen that dynamical performance of the EMSC is influenced by electromagnetic torque which depends on induced current in three-phase windings and excitation current in field winding. According to mathematical model of the PWM rectifier, current in three-phase windings is related to the modulation of the PWM rectifier. So output speed of EMSC can be regulated by excitation current in field winding and PWM rectifier modulation. Based on above analysis, efficient slip energy recovery of EMSC can be realized by PWM rectifier modulation. The principles of modulation are that input voltage and input current of PWM rectifier is in-phase and input current is sinusoidal to eliminate high-frequency harmonic components. To realize the phase synchronization between input current and input voltage of PWM rectifier, direct-axis component of current in three-phase windings should be adjusted to zero.

Mathematical model of the PWM rectifier is simplified as follows.

$$\begin{cases} L\dfrac{\mathrm{d}i_d}{\mathrm{d}t} = u_d - Ri_d - u_d' + L\omega i_q \\ L\dfrac{\mathrm{d}i_q}{\mathrm{d}t} = u_q - Ri_q - u_q' - L\omega i_d \end{cases} \tag{8}$$

Where u_d' is direct-axis component of input voltage of rectifier bridge, u_q' is quadrature-axis component of input voltage of rectifier bridge.

From above expressions, it can be seen that direct-axis component and quadrature-axis component of current in three-phase windings are coupled. To achieve current decoupling, feed forward control approach is proposed as follows.

$$\begin{cases} u_d'^* = -\left[K_{P1}(i_d^* - i_d) + K_{I1}\displaystyle\int (i_d^* - i_d)\mathrm{d}t\right] + L\omega i_q + u_d \\ u_q'^* = -\left[K_{P2}(i_q^* - i_q) + K_{I2}\displaystyle\int (i_q^* - i_q)\mathrm{d}t\right] - L\omega i_d + u_q \end{cases} \tag{9}$$

Where, $u_d'^*$ is desired direct-axis component of input voltage of rectifier bridge, $u_q'^*$ is desired quadrature - axis component of input voltage of rectifier bridge, i_d^* is desired direct-axis component of current in three-phase windings, i_q^* is desired quadrature-axis component of current in

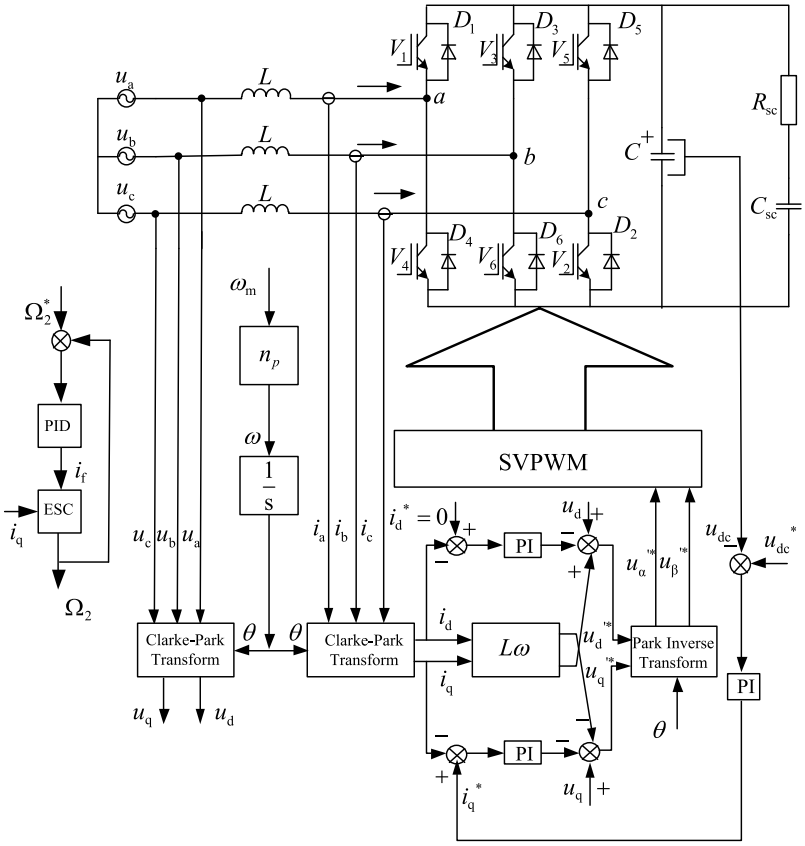

FIGURE 7. Control sketch of energy-regenerative EMSC.

three-phase windings, K_{P1} is proportional coefficient of the PI controller to control i_d, K_{I1} is integral coefficient of the PI controller to control i_d, K_{P2} is proportional coefficient of the PI controller to control i_q, K_{I2} is integral coefficient of the PI controller to control i_q.

By combining expression (8) and (9), the analytical equation is deduced as follows.

$$\begin{cases} L\dfrac{\mathrm{d}i_d}{\mathrm{d}t} = K_{P1}(i_d^* - i_d) + K_{I1}\displaystyle\int (i_d^* - i_d)\mathrm{d}t - Ri_d \\ L\dfrac{\mathrm{d}i_q}{\mathrm{d}t} = K_{P2}(i_q^* - i_q) + K_{I2}\displaystyle\int (i_q^* - i_q)\mathrm{d}t - Ri_q \end{cases} \tag{10}$$

Where, i_d^* is set as zero to realize phase synchronization of current and voltage in three-phase windings. i_q^* is presented in the following expression to ensure that voltage of DC side after rectification is steady.

$$i_q^* = K_{P3}(u_{dc}^* - u_{dc}) + K_{I3}\int (u_{dc}^* - u_{dc})\mathrm{d}t \tag{11}$$

Where, K_{P3} is the proportional coefficient of the PI controller to control u_{dc}, K_{I3} is the integral coefficient of the PI controller to control u_{dc}.

In this case, kinematic equation of the EMSC is transformed into following equation.

$$\frac{3}{2}n_p M_{sf} i_q i_f = J_2\frac{\mathrm{d}\Omega_2}{\mathrm{d}t} + B_2\Omega_2 + T_L \tag{12}$$

It can be seen that output speed of EMSC is closely relative to quadrature-axis component of current in three-phase windings and excitation current in field winding from above expression. Quadrature-axis component of current can be resolved by expression (10) and (11). Excitation current is expressed by following equation to ensure that output speed of EMSC tracks the desired value in the case of load disturbance.

$$i_f = K_P(\Omega_2^* - \Omega_2) + K_I\int (\Omega_2^* - \Omega_2)\mathrm{d}t + K_D\frac{\mathrm{d}(\Omega_2^* - \Omega_2)}{\mathrm{d}t} \tag{13}$$

Where, Ω_2^* is desired mechanical angular velocity of inner rotor, K_P is the proportional coefficient of the PID controller to control Ω_2, K_I is the integral coefficient of the PID controller to control Ω_2, K_D is the differential coefficient of the PID controller to control Ω_2.

Through above analysis and synthesis, control sketch of energy-regenerative EMSC is presented in FIGURE 7.

Based on the principle of super capacitor, recycled energy in super capacitor is expressed as following expression.

$$\Delta E = \frac{1}{2}C_{sc}u_{sc}^2 - \frac{1}{2}C_{sc}u_{sc0}^2 \tag{14}$$

Where, ΔE is recycled energy in super capacitor, u_{sc} is terminal voltage of super capacitor, u_{sc0} is initial terminal voltage of super capacitor.

V. SIMULATION ANALYSIS

To investigate dynamic performance and energy recovery performance of the energy-regenerative EMSC, simulations are carried out. Simulation parameters are shown in TABLE. 2.

TABLE 2. Simulation parameters.

Parameters/Unit	Value
Inductance of filter inductor L/H	5e-2
Equivalent resistance of filter inductor and MOSFETs R/Ω	5e-1
Capacitance of super capacitor C_{sc}/F	165
Internal resistance of super capacitor R_{sc}/Ω	1e-2

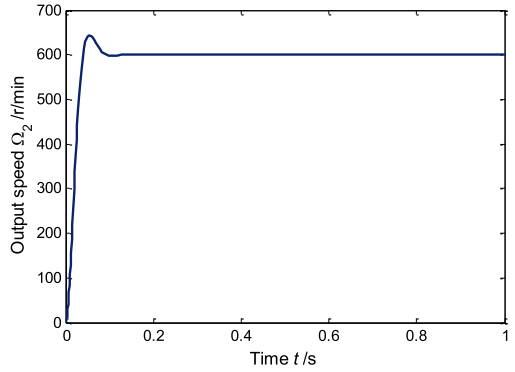

FIGURE 8. Output speed of EMSC by simulation.

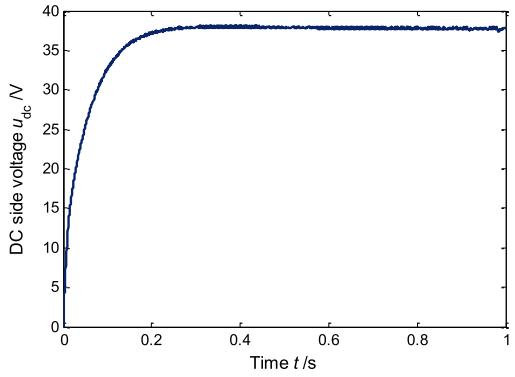

FIGURE 9. Voltage of DC side by simulation.

The simulation conditions are that input speed of EMSC is 1200 r/min, desired output speed is set as 600 r/min, and load torque on output shaft is 10 N·m. Simulation results are presented in FIGURE 8 to FIGURE 12. In FIGURE 8, output speed of the EMSC is quickly convergent to the desired value of 600 r/min after a slight overshoot. From FIGURE 9, it can be seen that voltage of DC side of PWM rectifier reaches steady state in a very short time. Simulation results of output speed and DC side voltage both demonstrate excellent dynamic performance of energy-regenerative EMSC.

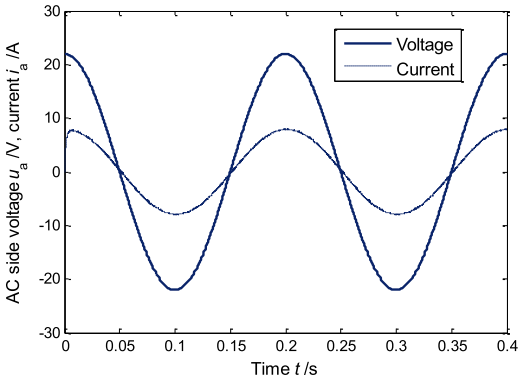

FIGURE 10. Voltage and current of AC side by simulation.

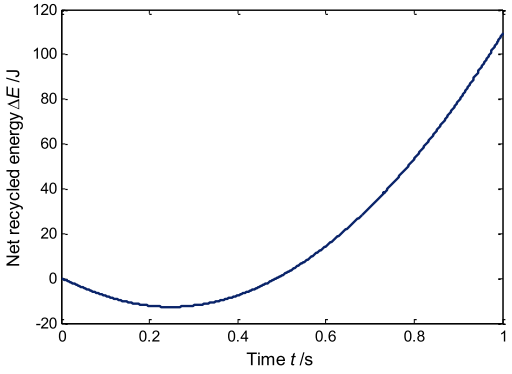

FIGURE 11. Net recycled energy by simulation.

In FIGURE 10, voltage and current of AC side of PWM rectifier are almost in same phase, which indicates approximate unity power factor of the energy-regenerative apparatus. Simulation of net recycled energy that is the difference between recycled energy in super capacitor and excitation energy is implemented. The result as shown in FIGURE 11 indicates that recycled energy is less than excitation energy at the beginning, and then it increases fast as time goes on. The effect of initial terminal voltage of the super capacitor on net recycled energy is also investigated. The simulation result is presented in FIGURE 12. It shows that net recycled energy

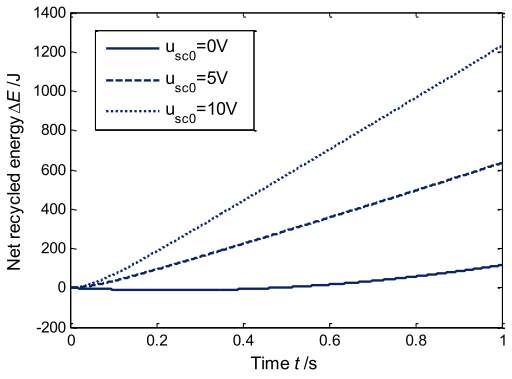

FIGURE 12. Net recycled energy with different initial terminal voltage.

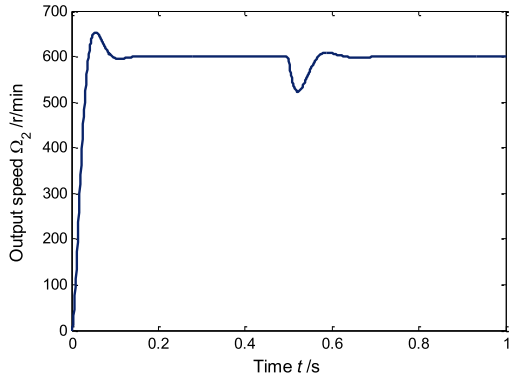

FIGURE 13. Output speed of EMSC under load disturbance condition by simulation.

increases observably with initial terminal voltage of super capacitor, which demonstrates that the energy-regenerative apparatus can substantially recycle slip energy of EMSC.

During the simulation, load torque of the EMSC is stepped from 10 N·m to 15 N·m to validate anti-disturbance performance of the proposed control strategy. The simulation result in FIGURE 13 shows that output speed of EMSC decreases by 80 r/min at the time of 0.5 seconds and then returns to 600 r/min in a short time.

VI. EXPERIMENT VERIFICATION

The test bench and test system of energy-regenerative EMSC are developed to verify the proposed control strategy by experiment. The test bench consists of variable frequency motor, torque-speed sensors, EMSC, magnetic powder dynamometer and control cabinet as shown in FIGURE 14.

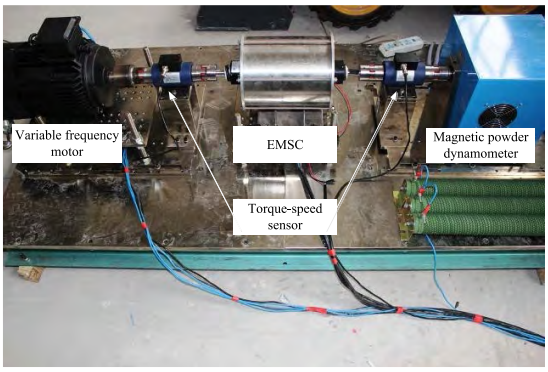

FIGURE 14. Test bench of energy-regenerative EMSC.

Test system consists of controller, PWM rectifier, super capacitor, current sensor, acquisition instrument and oscilloscope as shown in FIGURE 15. The test conditions are that output speed of variable frequency motor is set as 1200 r/min, load torque of the EMSC is set as 10 N·m, desired output speed of the EMSC is set as 600 r/min. In the experiment voltage and current of three-phase windings, field winding and super capacitor are collected by the oscilloscope; output speed of EMSC is acquired by the acquisition instrument.

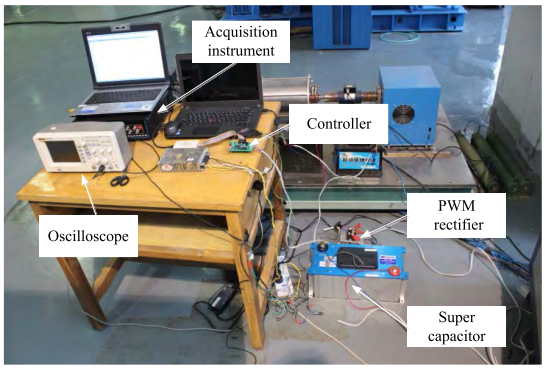

FIGURE 15. Test system of energy-regenerative EMSC.

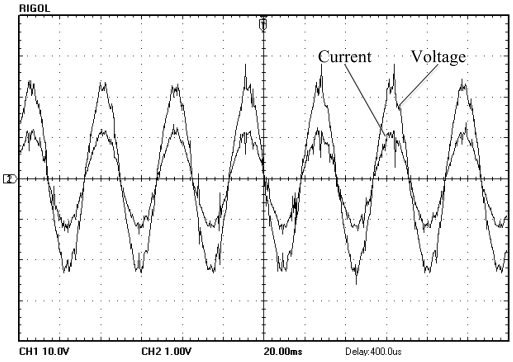

FIGURE 16. Voltage and current of AC side by experiment.

Test results are presented in FIGURE 16, FIGURE 17 and TABLE. 3.

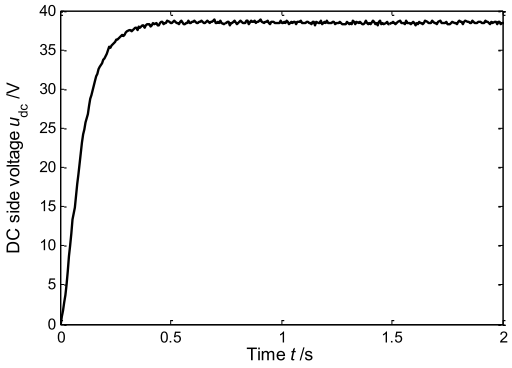

FIGURE 17. Voltage of DC side by experiment.

It can be seen from FIGURE 16 that input voltage and input current of PWM rectifier are almost in-phase, and input current contains few of high-frequency harmonic components, which demonstrates that the control strategy functions effectively and efficiently. In FIGURE 17, DC side voltage of PWM rectifier reaches the steady value of 38.5 V at the time of 0.6 seconds, which is consistent with the one in the simulation. The stabilization time of DC side voltage in the experiment is a bit longer than the one in the simulation since factors such as hysteresis and friction are not

TABLE 3. Results of bentch test.

Category	Parameters/Unit	Value
Input of EMSC	Input speed Ω_1 / r/min	1210
	Input torque T_1 /N·m	10.5
	Input power P_1 /W	1329
Output of EMSC	Output speed Ω_2 / r/min	605
	Output torque T_2 /N·m	9.9
	Output power P_2 /W	627
Excitation of EMSC	Excitation voltage u_f /V	9.4
	Excitation current i_f /A	5.5
	Excitation power P_f /W	52
Super capacitor	Charging voltage u_{sc} /V	38.5
	Charging current i_{sc} /A	16.4
	Recycled power P_{sc} /W	631

considered in the simulation. Test results of torque and speed of EMSC, excitation voltage and current of field winding, charging voltage and current of super capacitor are presented in TABLE. 3. Input power, output power, excitation power and recycled power is obtained from control cabinet as shown in TABLE. 3.

Based on input power and output power, slip power of EMSC can be calculated by following equation.

$$\Delta P = P_1 - P_2 = 702 \text{ W} \tag{15}$$

Net recycled power in the super capacitor is expressed as following.

$$P_r = P_{sc} - P_f = 579 \text{ W} \tag{16}$$

So energy-saving rate of EMSC can be obtained by following expression.

$$\eta = \frac{P_r}{\Delta P} = 82.5\% \tag{17}$$

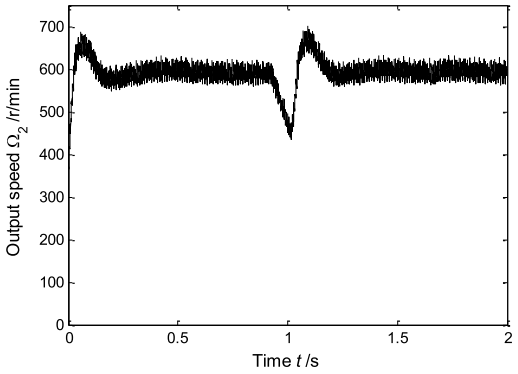

FIGURE 18. Output speed of EMSC under load disturbance condition by experiment.

Just like the simulation, load torque of EMSC is stepped from 10 N·m to 15 N·m in the experiment. Test result in FIGURE 18 shows that output speed of EMSC decends to 450 r/min at the time of one second, then it increases rapidly and returns to the initial value after a fluctuation about 100 r/min in a short time, which demonstrates the robust anti-disturbance capability of the energy-regenerative EMSC with the field-oriented control strategy.

VII. CONCLUSIONS

The novel energy-regenerative EMSC was developed for slip energy recovery. In this paper, the configuration of the EMSC was constructed; the mathematical models were built; the field-oriented control strategy was designed; simulations and experiments were carried out for the validation. Based on the investigated results, the following conclusions can be drawn.

(1) The mathematical model of the EMSC under synchronously rotating coordinate system was obtained and the integrated model of EMSC and PWM rectifier was initiatively deduced. The consistency of simulation and experiment results indicates that mathematical model of the EMSC has high accuracy.

(2) From the mathematical model of PWM rectifier, it can be seen that direct-axis component and quadrature-axis component of current in three-phase windings are coupled. To achieve the current decoupling, feed forward control approach was proposed.

(3) The simulation and experiment results both demonstrated excellent dynamical performance and robust anti-disturbance capability of the energy-regenerative EMSC with field-oriented control strategy.

(4) Based on the proposed control strategy, unity power factor of the energy recovery apparatus was realized. Test results showed that energy recovery efficiency of the energy-regenerative EMSC reached 82.5%, which demonstrated that transmission efficiency of EMSC was highly improved.

REFERENCES

[1] X. Yang, G. F. Gong, H. Yang, L. Jia, and J. Zhou, "An investigation in performance of a variable-speed-displacement pump-controlled motor system," *IEEE/ASME Trans. Mechatronics*, vol. 22, no. 2, pp. 647–656, Apr. 2017, doi: 10.1109/TMECH.2016.2544440.

[2] E. Al-Bassam and R. Alasseri, "Measurable energy savings of installing variable frequency drives for cooling towers' fans, compared to dual speed motors," *Energy Buildings*, vol. 67, pp. 261–266, Dec. 2013, doi: 10.1016/j.enbuild.2013.07.081.

[3] A. Khatkhate, S. Gupta, A. Ray, and R. Patankar, "Anomaly detection in flexible mechanical couplings via symbolic time series analysis," *J. Sound Vib.*, vol. 311, pp. 608–622, Apr. 2008, doi: 10.1016/j.jsv.2007.09.046.

[4] W. Li, Z. Zhou, B. Zhang, and Y. Xiao, "A micro-coupling for micro mechanical systems," *Chin. J. Mech. Eng.*, vol. 29, no. 3, pp. 571–578, 2016, doi: 10.3901/CJME.2016.0115.009.

[5] F. Xie, D. Wu, Y. Tong, B. Zhang, and J. Zhu, "Effects of structural parameters of oil groove on transmission characteristics of hydro-viscous clutch based on viscosity-temperature property of oil film," *Ind. Lubrication Tribol.*, vol. 69, no. 5, pp. 690–700, 2017, doi: 10.1108/ILT-12-2015-0207.

[6] B. Murty, S. Gopalakrishnan, C. Namuduri, K. Shoemaker, S. Opiteck, and B. Bezzina, "Magneto-rheological coupling based hydraulic power steering: Low-cost solution for fuel economy improvement," *SAE Int. J. Passenger Cars–Mech. Syst.*, vol. 2, no. 1, pp. 219–228, 2009, doi: 10.4271/2009-01-0046.

[7] T. Lubin, S. Mezani, and A. Rezzoug, "Simple analytical expressions for the force and torque of axial magnetic couplings," *IEEE Trans. Energy Convers.*, vol. 27, no. 2, pp. 536–546, Jun. 2012, doi: 10.1109/TEC.2012.2183372.

[8] T. Lubin, S. Mezani, and A. Rezzoug, "Experimental and theoretical analyses of axial magnetic coupling under steady-state and transient operations," *IEEE Trans. Ind. Electron.*, vol. 61, no. 8, pp. 4356–4365, Aug. 2014, doi: 10.1109/TIE.2013.2266087.

[9] R. You, B. Barahona, J. Chai, and N. A. Cutululis, "Frequency support capability of variable speed wind turbine based on electromagnetic coupler," *Renew. Energy*, vol. 74, pp. 681–688, Feb. 2015, doi: 10.1016/j.renene.2014.08.072.

[10] J. Hao-Bin, T. Bin, X. Zhe, and G. Guo-Qing, "Electromagnetic and torque characteristics of electromagnetic slip coupling applied to hydraulic power steering system for heavy-duty vehicles," *J. Comput. Theor. Nanosci.*, vol. 12, no. 6, pp. 1069–1075, 2015, doi: 10.1166/jctn.2015.3852.

[11] B. Dolisy, S. Mezani, T. Lubin, and J. Lévêque, "A new analytical torque formula for axial field permanent magnets coupling," *IEEE Trans. Energy Convers.*, vol. 30, no. 3, pp. 892–899, Sep. 2015, doi: 10.1109/TEC.2015.2424159.

[12] H.-B. Kang and J.-Y. Choi, "Parametric analysis and experimental testing of radial flux type synchronous permanent magnet coupling based on analytical torque calculations," *J. Elect. Eng. Technol.*, vol. 9, no. 3, pp. 926–931, 2014, doi: 10.5370/JEET.2014.9.3.926.

[13] A. Canova and B. Vusini, "Design of axial eddy-current couplers," *IEEE Trans. Ind. Appl.*, vol. 39, no. 3, pp. 725–733, May/Jun. 2003, doi: 10.1109/TIA.2003.811783.

[14] H. K. Razavi and M. U. Lamperth, "Eddy-current coupling with slotted conductor disk," *IEEE Trans. Magn.*, vol. 42, no. 3, pp. 405–410, Mar. 2006, doi: 10.1109/TMAG.2005.862762.

[15] Z. Mouton and M. J. Kamper, "Modeling and optimal design of an eddy current coupling for slip-synchronous permanent magnet wind generators," *IEEE Trans. Ind. Electron.*, vol. 61, no. 7, pp. 3367–3376, Jul. 2014, doi: 10.1109/TIE.2013.2282602.

[16] H. Nian, C. Wu, and P. Cheng, "Direct resonant control strategy for torque ripple mitigation of DFIG connected to DC link through diode rectifier on stator," *IEEE Trans. Power Electron.*, vol. 32, no. 9, pp. 6936–6945, Sep. 2017, doi: 10.1109/TPEL.2016.2630710.

[17] S. Ebrahimi, N. Amiri, H. Atighechi, L. Wang, and J. Jatskevich, "Verification of parametric average-value model of thyristor-controlled rectifier systems for variable-frequency wind generation systems," *IEEE Trans. Energy Convers.*, vol. 31, no. 1, pp. 401–403, Mar. 2016, doi: 10.1109/TEC.2015.2484065.

[18] N. Holonyak, "The silicon p-n-p-n switch and controlled rectifier (thyristor)," *IEEE Trans. Power Electron.*, vol. 16, no. 1, pp. 8–16, Jan. 2001, doi: 10.1109/63.903984.

[19] J. Wang, D. Xu, B. Wu, and Z. Luo "A low-cost rectifier topology for variable-speed high-power PMSG wind turbines," *IEEE Trans. Power Electron.*, vol. 26, no. 8, pp. 2192–2200, Aug. 2011, doi: 10.1109/TPEL.2011.2106143.

[20] A. Monpapassorn, K. Dejhan, and F. Cheevasuvit, "CMOS dual output current mode half-wave rectifier," *Int. J. Electron.*, vol. 88, no. 10, pp. 1073–1084, 2001, doi: 10.1080/00207210110071242.

[21] J. R. Rodriguez, J. W. Dixon, J. R. Espinoza, J. Pontt, and P. Lezana, "PWM regenerative rectifiers: State of the art," *IEEE Trans. Ind. Electron.*, vol. 52, no. 1, pp. 5–22, Feb. 2005, doi: 10.1109/TIE.2004.841149.

[22] B.-R. Lin, "Analysis and implementation of a three-level PWM rectifier/inverter," *IEEE Trans. Aerosp. Electron. Syst.*, vol. 36, no. 3, pp. 948–956, Jul. 2000, doi: 10.1109/7.869514.

[23] K. Zeb, Z. Ali, K. Saleem, W. Uddin, M. A. Javed, and N. Christofides, "Indirect field-oriented control of induction motor drive based on adaptive fuzzy logic controller," *Elect. Eng.*, vol. 99, no. 3, pp. 803–815, 2017, doi: 10.1007/s00202-016-0447-5.

[24] X. Qiu, W. Zhao, Q. Chen, and D. Xu, "Mover field oriented control of linear permanent-magnet Vernier motor considering loss minimization," *J. Elect. Eng. Technol.*, vol. 12, no. 3, pp. 1114–1123, 2017, doi: 10.5370/JEET.2017.12.3.1114.

[25] O. Wallmark, S. Lundberg, and M. Bongiorno, "Input admittance expressions for field-oriented controlled salient PMSM drives," *IEEE Trans. Power Electron.*, vol. 27, no. 3, pp. 1514–1520, Mar. 2012, doi: 10.1109/TPEL.2011.2118231.

[26] A. K. Jain and V. T. Ranganathan, "Modeling and field oriented control of salient pole wound field synchronous machine in stator flux coordinates," *IEEE Trans. Ind. Electron.*, vol. 58, no. 3, pp. 960–970, Mar. 2011, doi: 10.1109/TIE.2010.2048295.

[27] M. Pucci, "Direct field oriented control of linear induction motors," *Electr. Power Syst. Res.*, vol. 89, pp. 11–22, Aug. 2012, doi: 10.1016/j.epsr.2012.01.012.

[28] J. F. Khan, S. M. A. Bhuiyan, K. M. Rahman, and G. V. Murphy, "Space vector PWM for a two-phase VSI," *Int. J. Elect. Power Energy Syst.*, vol. 51, pp. 265–277, Oct. 2013, doi: 10.1016/j.ijepes.2013.02.029.

[29] A. Bouafia, J.-P. Gaubert, and F. Krim, "Design and implementation of predictive current control of three-phase PWM rectifier using space-vector modulation (SVM)," *Energy Convers. Manage.*, vol. 51, pp. 2473–2481, Dec. 2010, doi: 10.1016/j.enconman.2010.05.010.

[30] C. Pan, L. Chen, L. Chen, C. Huang, and M. Xie, "Research on energy management of dual energy storage system based on the simulation of urban driving schedules," *Int. J. Elect. Power Energy Syst.*, vol. 44, no. 1, pp. 37–42, 2013, doi: 10.1016/j.ijepes.2012.07.025.

[31] N. Devillers, M.-C. Péra, D. Bienaimé, and M.-L. Grojo, "Influence of the energy management on the sizing of electrical energy storage systems in an aircraft," *J. Power Sources*, vol. 270, pp. 391–402, Dec. 2014, doi: 10.1016/j.jpowsour.2014.07.113.

[32] X. Zhang, Z. Zhang, H. Pan, W. Salman, Y. Yuan, and Y. Liu, "A portable high-efficiency electromagnetic energy harvesting system using supercapacitors for renewable energy applications in railroads," *Energy Convers. Manage.*, vol. 118, pp. 287–294, Jun. 2016, doi: 10.1016/j.enconman.2016.04.012.

[33] P. Sharma and T. S. Bhatti, "A review on electrochemical double-layer capacitors," *Energy Convers. Manage.*, vol. 51, pp. 2901–2912, Dec. 2010, doi: 10.1016/j.enconman.2010.06.031.

[34] X. Sun, L. Chen, Z. Yang, and H. Zhu, "Analysis of inductance characteristics for a bearingless permanent magnet synchronous motor," *Elect. Eng.*, vol. 95, no. 23, pp. 277–286, 2013, doi: 10.1007/s00202-012-0262-6.

BIN TANG received the B.S. degree in electronics and information engineering, and the M.S. and Ph.D. degrees in vehicle engineering from Jiangsu University, Zhenjiang, China, in 2007, 2011, and 2015, respectively.

He is currently an Associate Professor with the Automotive Engineering Research Institute, Jiangsu University. His research interests include automobile handling dynamics and control, intelligent steering, and drive control.

YINGQIU HUANG received the B.S. degree in vehicle engineering from Jiangsu University, Zhenjiang, China, in 2017.

He is currently pursuing the master's degree with the School of Automotive and Traffic Engineering, Jiangsu University, majored in vehicle engineering.

DI ZHANG received the B.S. degree in automobile service engineering from Qilu University of Technology, Jinan, China, in 2017.

She is currently pursuing the master's degree with the School of Automotive and Traffic Engineering, Jiangsu University, Zhenjiang, China, majored in vehicle engineering.

HAOBIN JIANG received the B.S. degree from Nanjing Agricultural University, Nanjing, China, in 1991, and the M.S. and Ph.D. degrees from Jiangsu University, Zhenjiang, China, in 1994 and 2000, respectively, all in mechanical engineering.

He is currently a Professor with the School of Automotive and Traffic Engineering, Jiangsu University. His research interests include vehicle dynamics performance analysis and electronic control technologies for vehicles.

YINGFENG CAI received the B.S., M.S., and Ph.D. degrees from the School of Instrument Science and Engineering, Southeast University, Nanjing, China.

She is currently a Professor in transportation engineering with the Automotive Engineering Research Institute, Jiangsu University. Her research interests include computer vision, intelligent transportation systems, and intelligent automobiles.

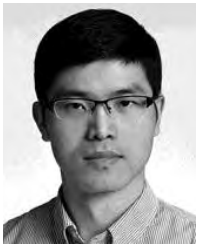

XIAODONG SUN received the B.S. degree in electrical engineering, and the M.S. and Ph.D. degrees in control engineering from Jiangsu University, Zhenjiang, China, in 2004, 2008, and 2011, respectively.

He is currently a Professor with the Automotive Engineering Research Institute, Jiangsu University. From 2014 to 2015, he was a Visiting Scholar with the School of Electrical, Mechanical, and Mechatronic Systems, University of Technology Sydney, Sydney, Australia. His areas of interests include electrical machines and drives, drives and control for electric vehicles, and intelligent control.